Taylor & Francis
Taylor & Francis Group

Journal of Electromagnetic Waves and Applications

ISSN: (Print) (Online) Journal homepage: https://www.tandfonline.com/loi/tewa20

A high gain circularly polarized 2 × 2 antenna array based on the spoof surface plasmon polariton and spoof localized surface plasmon

Qian-Qian Li & Hai-Feng Zhang

To cite this article: Qian-Qian Li & Hai-Feng Zhang (2023): A high gain circularly polarized 2 × 2 antenna array based on the spoof surface plasmon polariton and spoof localized surface plasmon, Journal of Electromagnetic Waves and Applications, DOI: 10.1080/09205071.2023.2234381

To link to this article: https://doi.org/10.1080/09205071.2023.2234381

JOURNAL OF ELECTROMAGNETIC WAVES AND APPLICATIONS
https://doi.org/10.1080/09205071.2023.2234381

Taylor & Francis
Taylor & Francis Group

A high gain circularly polarized 2 × 2 antenna array based on the spoof surface plasmon polariton and spoof localized surface plasmon

Qian-Qian Li and Hai-Feng Zhang

College of Electronic and Optical Engineering & College of Flexible Electronics (Future Technology), Nanjing University of Posts and Telecommunications, Nanjing, People's Republic of China

ABSTRACT

Two circularly polarized (CP) 2 × 2 array antennas based on the spoof surface plasmon polariton (SPP) and spoof localized surface plasmon (LSP) are proposed. The antenna I is fed by a feed network to increase the axial-ratio (AR) bandwidth. The spoof SPP and spoof LSP are introduced to increase the gain through energy localization, and the structure can suppress the cross-polarization to a certain extent and obtain a wider axial-ratio beamwidth. In addition, the electromagnetic band gap (EBG) is used to suppress surface waves to further increase the gain. The size of antenna I is 1.27λg × 1.27λg × 0.18λg. The impedance bandwidth and the AR bandwidth of antenna I are 72% (3.15–6.75 GHz) and 55% (3.97–6.72 GHz), respectively, and the peak gain is 11.11 dBi. The antenna II optimizes the distance between the two substrates according to antenna I to further increase the gain.

ARTICLE HISTORY
Received 28 May 2022
Accepted 4 July 2023

KEYWORDS
Spoof surface plasmon polariton; spoof localized surface plasmon; feed network; circularly polarized antenna array; electromagnetic band gap

1. Introduction

In recent years, circularly polarized (CP) antennas have been used more and more because of their ability to minimize multipath interference and polarization mismatch. With the development of communication technology, the requirements for communication capacity have become higher, so the demand for broadband antennas is increasing, while the traditional single CP patch antenna usually limits the AR bandwidth. Therefore, antenna arrays are increasingly used to obtain higher gain and wider bandwidth [1].

The feed network is considered to be one of the most effective means to improve the CP bandwidth in the antenna array. Therefore, a simple feed network matched by impedance transformation is proposed [2–5]. However, this method cannot obtain a stable 90° phase difference, resulting in only a narrow axial-ratio (AR) bandwidth. A T-structure sequential-phase feed network is also widely used [6,7], but still did not obtain a wide AR bandwidth due to its unbalanced power distribution and unstable phase difference. Therefore, Wilkinson power splitters and phase shifters are applied to the feed network to obtain a balanced

CONTACT Hai-Feng Zhang hanlor@163.com College of Electronic and Optical Engineering & College of Flexible Electronics (Future Technology), Nanjing University of Posts and Telecommunications, Nanjing 210023, People's Republic of China

power distribution and constant phase difference to improve the AR bandwidth [8–11]. In recent years, the electromagnetic band gap (EBG) structure has been used more and more in antennas [12–14]. EBG is a periodic structure used to suppress the propagation of harmonics and electromagnetic surface waves, and it also has the effect of anti-multipath interference. Combining this structure with a microstrip patch antenna can increase the gain of the antenna.

Surface plasmon polariton (SSP) has also attracted widespread attention in recent years. SPP is collective oscillations that occur after the interaction of free electrons on a metal surface and an incident wave. However, it is only effective in the optical frequency band and cannot be used in the microwave frequency band. For this reason, researchers have done a lot of research on artificial electromagnetic materials and realized spoof SPP that can imitate the characteristics of SPP [15–17]. Spoof SPP is formed by etching periodic square grooves on the metal surface, and electromagnetic waves are coupled to these etched square grooves [18]. The plasma resonance frequency of the metal is reduced due to the influence of the whole structure so that it can be achieved in the microwave frequency band. The spoof localized surface plasmon (LSP) is also widely used in the realization of the microwave frequency band [19–21]. Spoof LSP etches periodic grooves on the metal closed surface to increase the penetration of electromagnetic waves on the metal surface, thereby generating LSP resonance. However, most of the improvement techniques for antenna performance using Spoof SPP and Spoof LSP are still focused on beam scanning. This article will utilize the constraint ability of Spoof SPP and Spoof LSP on electromagnetic waves to enhance the antenna gain.

In this paper, two broadband CP 2×2 array antennas based on spoof SSP and spoof LSP are proposed. The antenna I is fed by the feed network to the radiation patche, and an EBG structure is added to suppress surface waves to increase gain. In addition, the antenna combines spoof SPP and spoof LSP to localize the energy to achieve the effect of further enhancing the gain. The impedance bandwidth and AR bandwidth of antenna I are 72% (3.15–6.75 GHz) and 55% (3.97–6.72 GHz), respectively, and the peak gain is 11.11 dBi. The antenna II adjusts the height of the probes based on the antenna I to further increase the gain and combines with the spoof LSP to increase the AR bandwidth. The impedance bandwidth of the proposed antenna II is 71.8% (3.14–6.73 GHz), the measured AR bandwidth is 53.2% (4.10–6.76 GHz), and the peak gain is 12.05 dBi.

2. Antenna design

2.1. Simulation of antenna I

The antenna I have a double-layer structure, as shown in Figure 1(a), with an overall size of $1.27\lambda g \times 1.27\lambda g \times 0.18\lambda g$. The antenna is printed on the F4B ($\epsilon_r = 2.2$, $\tan\delta = 0.003$) substrate.

Figure 1(b) shows the geometry of the feed network. The input signal cannot only realize equal power distribution through the Wilkinson power divider but also realize the impedance transformation between the input and output ports. After the input signal is divided into two channels, the adjacent ports have a stable 90° phase difference through the microstrip line and the phase shifter respectively, to obtain a wider bandwidth. The phase difference of 90° is realized by a quarter-wavelength difference microstrip line, and

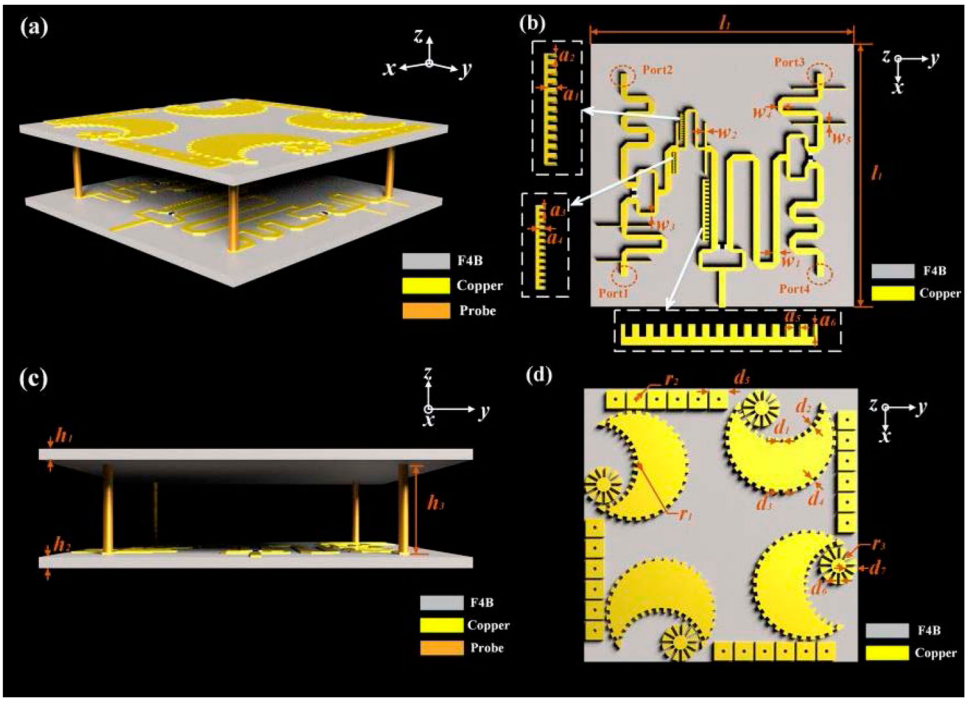

Figure 1. Geometry of the proposed antenna I: (a) structure of antenna I, (b) feed network, (c) side view, (d) top view.

the wavelength is calculated by Eq. (1) to be 47 mm [4].

$$\lambda_g = \frac{c}{f\sqrt{(\varepsilon_r + 1)/2}} \tag{1}$$

Figure 2 shows the s-parameters and phase of the feed network. Figure 2(a) shows that the output power of adjacent ports is relatively stable. Figure 2(b) shows that the phase difference between two adjacent ports can be maintained at about 90° between 3 and 7 GHz, some of the instability may be due to the mutual coupling between the microstrip lines. Figure 2(c) shows that the impedance bandwidth of the proposed feed network is 3.11–6.74 GHz. The feed network feeds the radiation patches through four probes, and this feeding method can be clearly seen from the side as shown in Figure 1(c). Figure 1(d) shows the top view of antenna I. The radiation patches of the proposed antenna adopt a crescent-shaped, that is, a small circle is subtracted from the circular radiation patch to introduce disturbance, and two degenerate modes are generated to realize CP. The parameters have been optimized and shown in Table 1.

The proposed antenna I is discussed in five steps, steps 1 and 2 are shown in Figure 3. The smooth crescent-shaped radiation patches are used in step 1, the structure is to separate two orthogonal modes by subtracting a small circle from a large circular patch, so the size of the crescent is a key parameter. From Figure 4(a), it can be seen that r_4 has little effect on $|S_{11}|$. Figure 4(b) shows the AR simulation results for different r_4 values. It can be seen that AR deteriorates around 4 GHz when r_4 is larger than 9 mm, while AR results are best and the high-frequency bandwidth is slightly wider when $r_4 = 9$ mm. Figure 4(c) shows that the

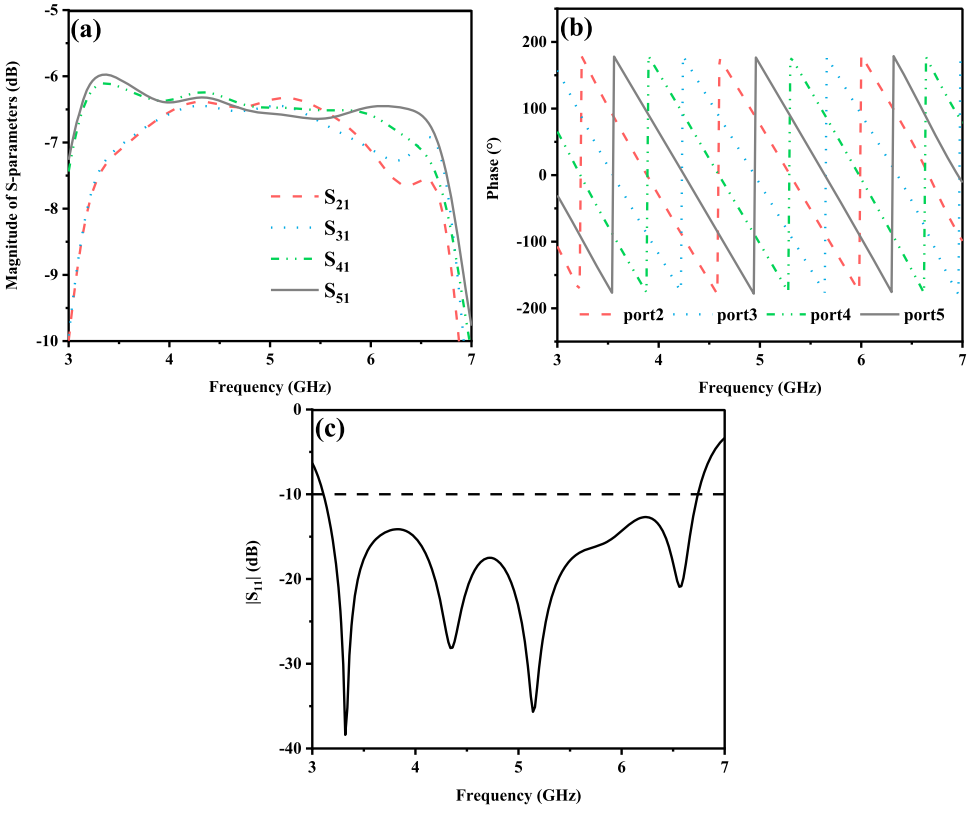

Figure 2. The simulated values of the proposed feed network: (a) power output of each port, (b) phase difference of each port, (c) $|S_{11}|$ of the feed network.

Table 1. Detailed dimensions.

Parameter	l_1	w_1	w_2	w_3	w_4	w_5	r_1	r_2	r_3	h_1	h_2
Value (mm)	60	1.5	0.5	0.84	1.1	0.2	12	0.4	4	0.5	0.5
Parameter	h_3	a_1	a_2	a_3	a_4	a_5	a_6	d_1	d_2	d_3	d_4
Value (mm)	8	0.5	0.3	0.2	0.3	0.5	0.9	1	1	1	0.74
Parameter	d_5	d_6	d_7	k_1	k_2	k_3	k_4	k_5	k_6	k_7	k_8
Value (mm)	4	0.7	2.5	2	4	1	1.5	0.55	0.7	0.4	0.5

peak gain of the antenna is highest when $r_4 = 9.5$ mm and $r_4 = 10$ mm, but at this point, the antenna AR deteriorates at around 4 GHz. The gain peak is close when $r_4 = 8.5$ mm and $r_4 = 9$ mm, while the gain peak is the lowest when $r_4 = 8$ mm. Due to the best AR at $r_4 = 9$ mm, r_4 is the most reasonable at 9 mm.

Figure 5 shows the AR, $|S_{11}|$ and gain of the antenna at different patch radii (r_1). It can be seen that AR will deteriorate when $r_1$is less than 12 mm, and it will also exceed 3 dB at around 6.2 GHz when r_1 is greater than 12 mm. This is because the magnitude of the two orthogonal degenerate modes is different due to the different sizes of the patches. Therefore, when $r_1 = 12$ mm is the most suitable, the AR bandwidth is 3.44–7.44 GHz and the relative bandwidth is 80%. Figure 5(b) shows the graph of $|S_{11}|$, from which it can be seen that the influence of r_1 on the overall trend of $|S_{11}|$ is not very large. However, the

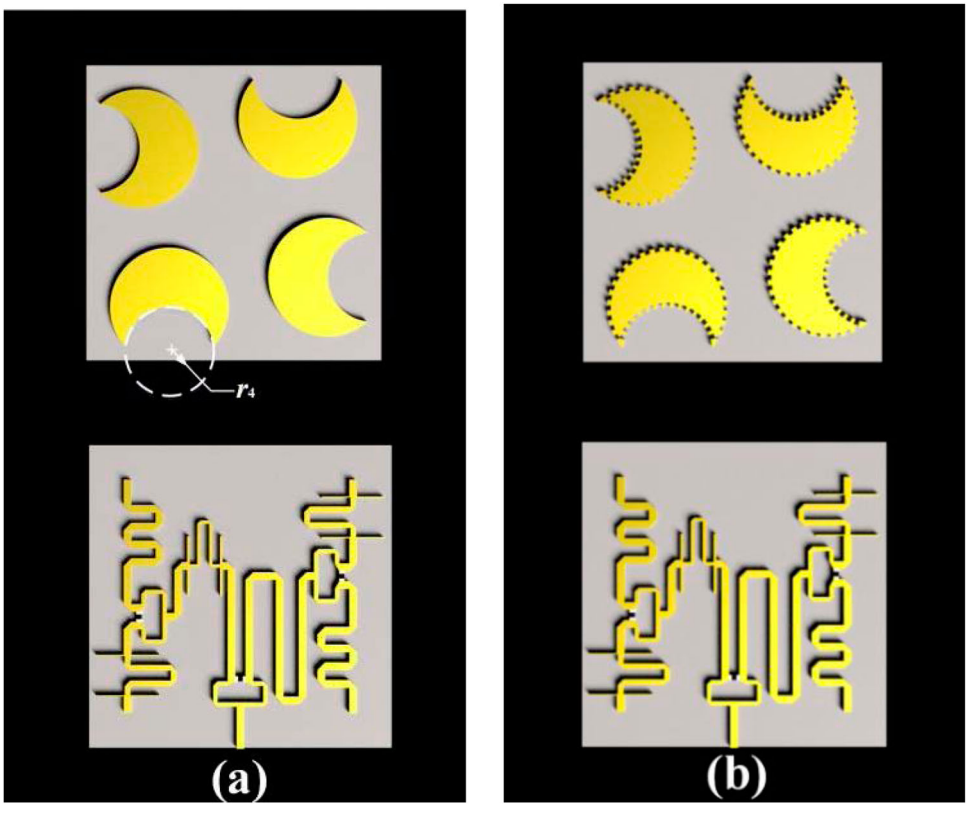

Figure 3. Antenna improvement steps: (a) step 1, (b) step 2.

impedance of high-frequency will deteriorate slightly when r_1 is larger than 12 mm, which is due to the impedance mismatch caused by the increase in the size of the radiation patches at this time. As shown in Figure 5(c), the gain shifts towards lower frequency as r_1 becomes larger, because the size of the radiation patches of the antenna is affected by the wavelength and thus changes the resonant frequency. In addition, the gain decreases when r_1 is greater than 12 mm. This is because when the patch is too large, the adjacent patches are very close, which makes the coupling serious and affects the gain.

In a word, the peak gain is 10.58 dBi when $r_1 = 12$ mm, but still cannot get a very high gain at this time. Therefore, spoof SPP is introduced based on step 1 to increase the gain of the antenna. Spoof SPP is formed by the electronic coupling resonance in the metal periodic groove, so as shown in step 2, the smooth radiation patches are changed to a zigzag shape. Periodic grooves are etched on the metal surface to limit the energy, thereby forming a field enhancement at the interface between the metal and the medium to increase the gain. Figure 6(a) shows that the peak gain at this time is 10.73 dBi, which is 0.15 dBi higher than step 1. However, AR is deteriorated to a certain extent at around 4 and 6.4 GHz due to the change of amplitude, and further optimization steps need to be proposed to solve this problem. But the $|S_{11}|$ of the two steps is not much different. To further verify the proposed spoof SPP, the current density is also simulated. Figure 6(a) shows that step 2 has the largest gain improvement at 6.4 GHz compared to step 1, so the current diagrams

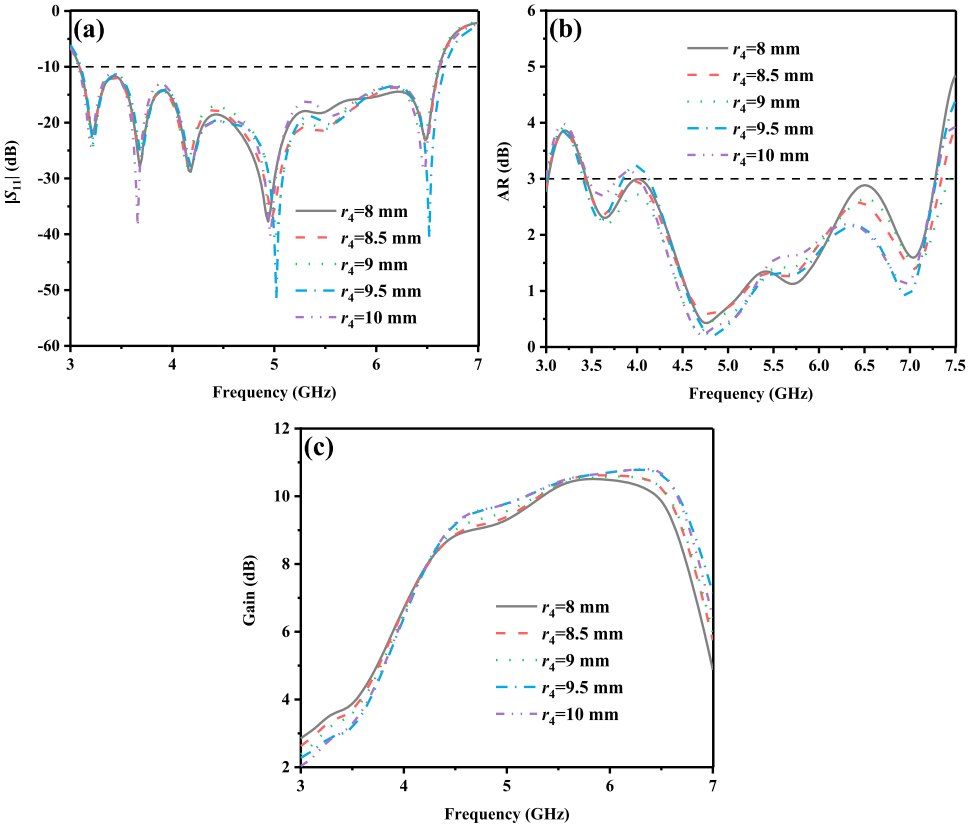

Figure 4. Simulate results for different r_4: (a) $|S_{11}|$, (b) AR, (c) gain.

of these two steps at this frequency are shown in Figure 7. It is evident that the edges of the crescent-shaped radiation patches have obvious localized effects after adding periodic grooves, which further confirms the effect of spoof SPP.

To improve the deteriorating AR and further increase the gain, steps 3–5 are shown in Figure 8. The spoof SPP surface wave will be firmly bound to the surface of the structure, which can greatly reduce the crosstalk between adjacent structures, and since it propagates on the metal surface, the dielectric loss can be reduced to a certain extent. Therefore, step 3 introduces spoof SPP into the feed network and uses its mode mismatch with the microstrip line to suppress crosstalk, thereby reducing the coupling of the microstrip line and improving the performance of the antenna. It can be seen from Figure 9(a) that the peak gain at this time is 11.05 dBi, which is 0.32 dBi higher than step 2. At this time, the AR deteriorated around 6.4 GHz in step 2 is improved, but still, more than 3 dB around 4 GHz, as shown in Figure 9(b). It can be seen from Figure 9(c) that this change has little effect on $|S_{11}|$. In step 4, the EBG is introduced, which suppresses the surface wave during transmission to avoid the resulting parasitic coupling and loss, and converts it into space radiation to increase the gain. As shown in Figure 9(a), the peak gain of step 4 is 11.13 dBi, which is 0.08 dBi higher than that of step 3. At this time, the AR around 4 GHz is also improved, and the structure does not have a big impact on the $|S_{11}|$.

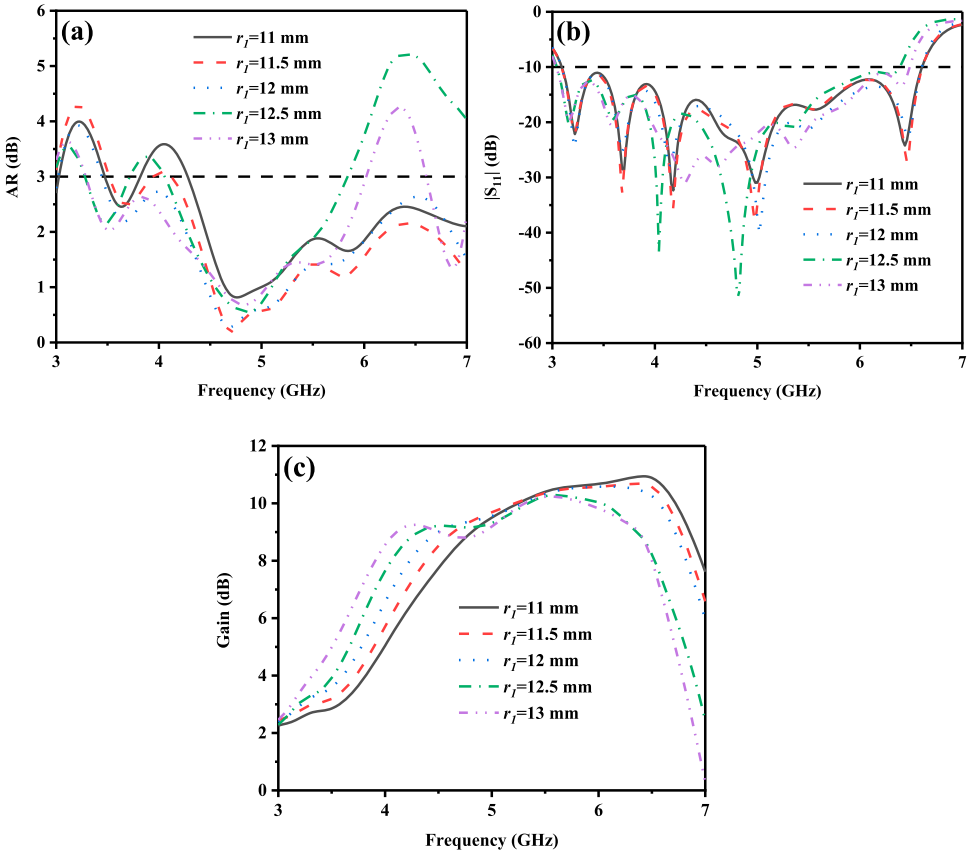

Figure 5. Simulate results for different r_1: (a) AR, (b) $|S_{11}|$, (c) gain.

Step 5 introduces the spoof LSP on the inside of the crescent-shaped radiation patches. The spoof LSP is to etch periodic grooves on the metal surface to increase the penetration of electromagnetic waves on the metal surface, resulting in the phenomenon of local surface plasmon resonance. This allows electromagnetic energy to be well confined to the surface, and field enhancement can be formed at the interface between the metal and the medium. In addition to increasing gain through local energy, this structure can also suppress cross-polarization to improve the axial-ratio beamwidth (ARBW). Figure 9(a) shows that the peak gain at this time reaches 11.20 dBi, which is 0.62 dBi higher than that of the initial step 1. It can be seen from Figure 10 that the ARBW is improved to a certain extent after adding the spoof LSP because the cross-polarization is suppressed. At 5.8 GHz, the 3-dB ARBW of step 5 can reach 50°, which is 12° better than step 4. At 6.3 GHz, the 3-dB ARBW of step 5 is over 63°, which is 33° better than that of step 4. The proposed antenna improves the two parameters of gain and 3-dB ARBW at the same time. The comparison between the above five steps is shown in Table 2.

Figure 11 shows the dispersion curves of the unit structures of the spoof SSP and spoof LSP described above. It can be seen that when the frequency is low, the dispersion curve of the unit structure is very close to the dispersion curve of the light. As the frequency

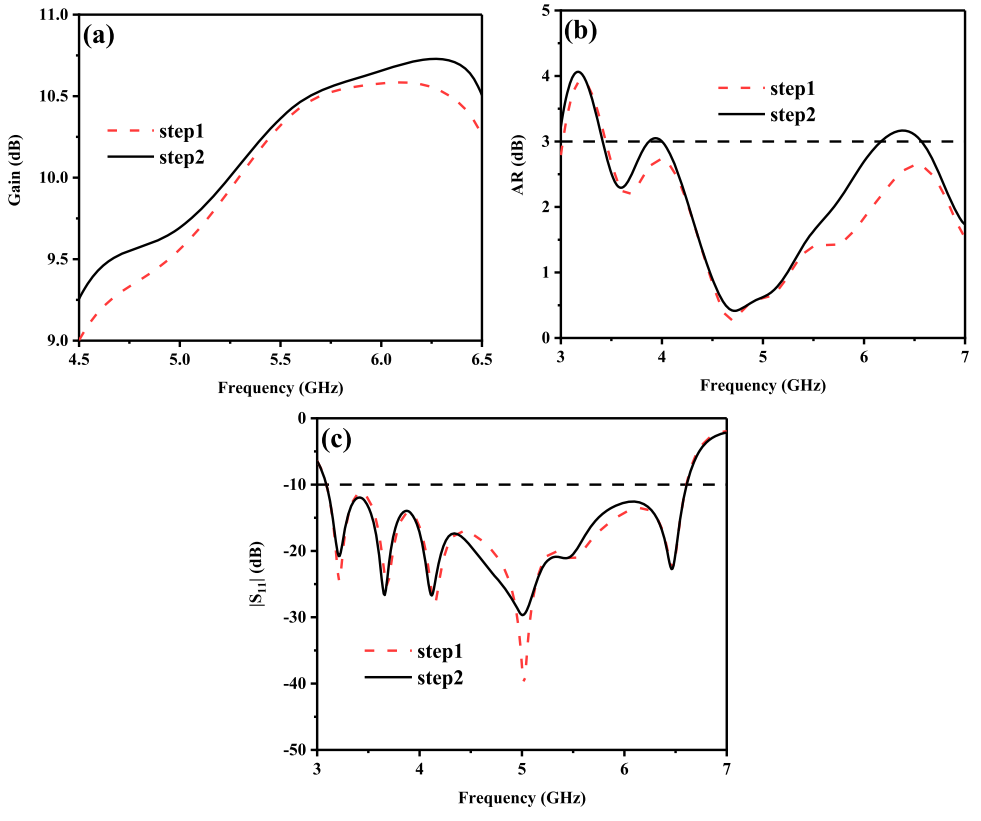

Figure 6. Comparison of step 1 and step 2: (a) gain, (b) AR, (c) $|S_{11}|$.

Table 2. Comparison of different steps.

Step	$\|S_{11}\|$BW (%)	AR BW (%)	Peak gain (dBi)	3-dB ARBW at 5.8 GHz (°)	3-dB ARBW at 6.3 GHz (°)
Step1	70.4	79.6	10.58	39	30
Step2	70.4	43.4	10.73	31	×
Step3	70.6	67.0	11.05	39	33
Step4	71	78.8	11.13	38	30
Step5	71.6	77.0	11.20	50	63

increases, the dispersion deviates more and more from the light and finally tends to be stable. When the dispersion curve tends to a straight line, the corresponding frequency is the cut-off frequency. The dispersion of the unit structure is on the right side of the light, so this structure is slow-wave transmission, causing electromagnetic waves to be confined in the plane. It can be seen from Figure 11 that when the other parameters remain unchanged and the depth of the groove gradually increases, the more the dispersion curve deviates from the light and the lower the cut-off frequency is. This shows that in the cut-off frequency range, the electromagnetic wave confinement ability of the metal surface becomes stronger as the depth of the groove increases. When the cut-off frequency is too low, it will cause too much energy to be localized in the radiation patches, which will affect the antenna's radiation and worsen the gain. Therefore, the cut-off frequency cannot be too low.

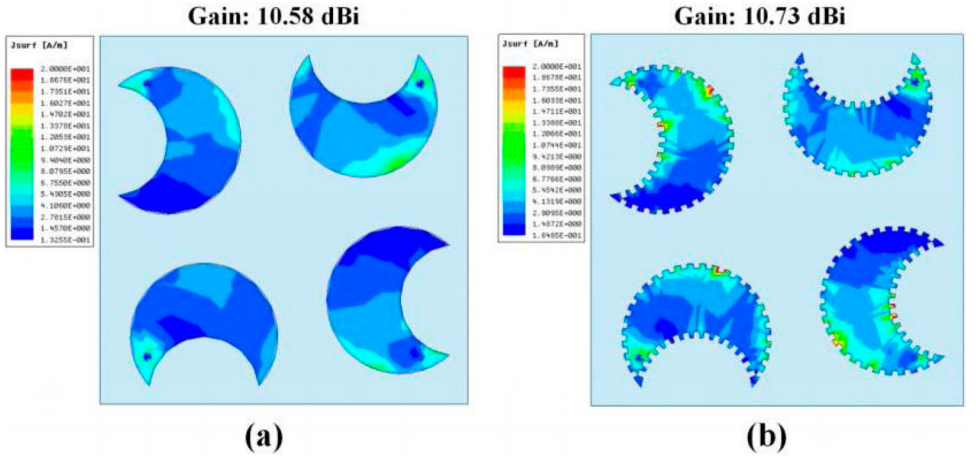

Figure 7. Current graph of radiation patches at 6.4 GHz: (a) step1, (b) step2.

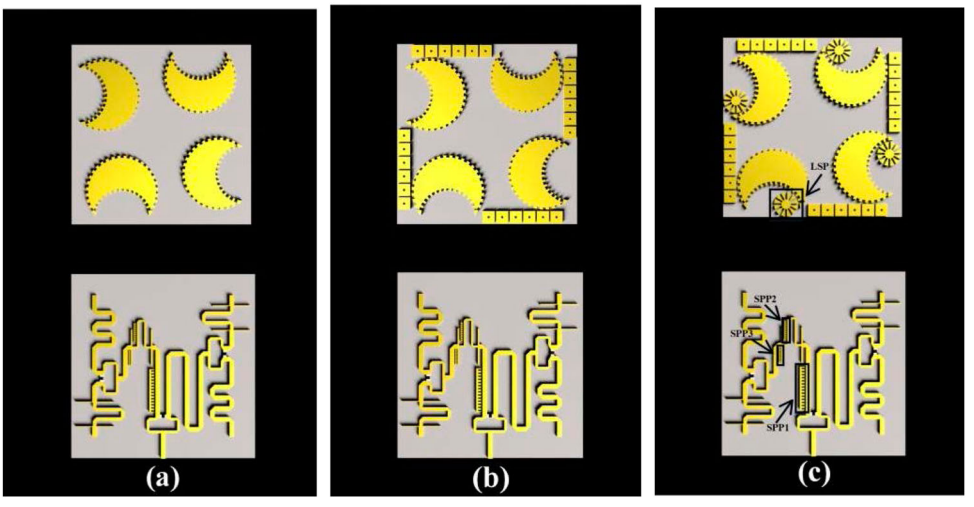

Figure 8. Antenna improvement steps: (a) step 3, (b) step 4, (c) step5.

The current distributions of different phases at 5 GHz are shown in Figure 12. The output ports are equal in magnitude and orthogonal to each other in the range of 0°, 90°, 180°, 270° due to feeding by the feed network. Furthermore, the antenna is left-hand circularly polarized (LHCP) since the current rotation direction is clockwise.

2.2. Simulation of antenna II

Since the proposed antenna has a two-layer structure, a parametric study on the distance between the two substrates is performed. Figure 13(a) shows the $|S_{11}|$ of the upper and lower substrates at different heights. When $h_3 = 4$ mm and $h_3 = 10$ mm, the $|S_{11}|$ will deteriorate at around 3.5 and 6.2 GHz, respectively. This is because the distance between

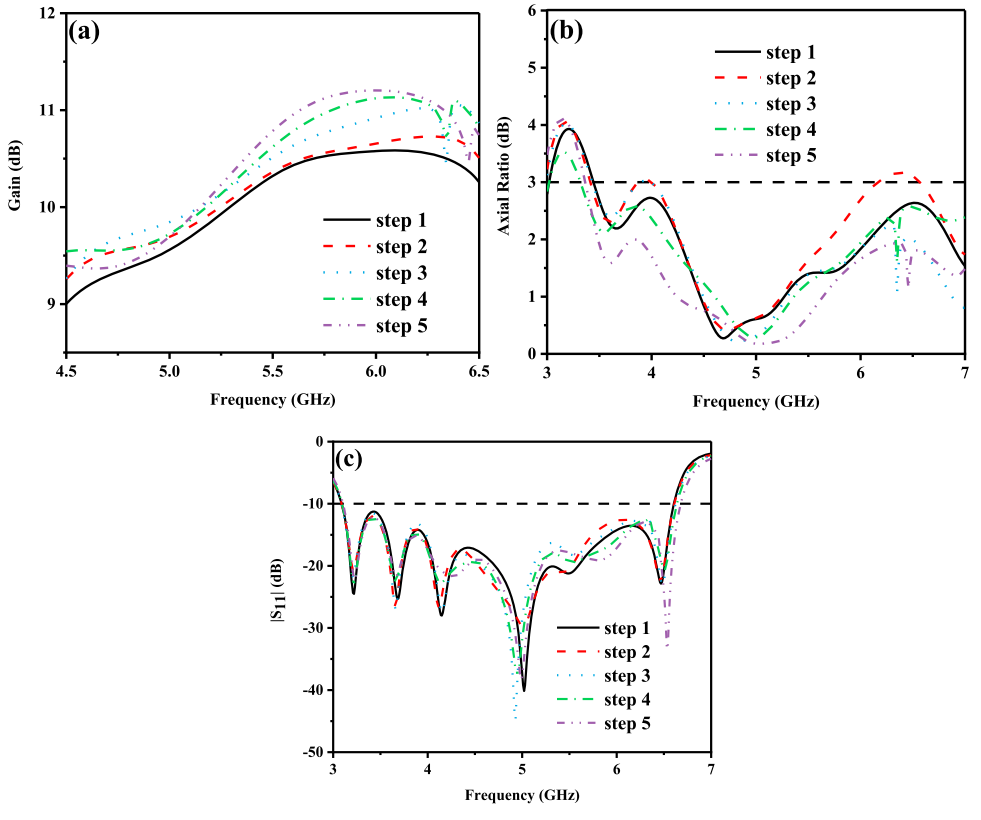

Figure 9. Simulation curve of the five design steps of the antenna I: (a) Gain, (b) AR, (c) $|S_{11}|$.

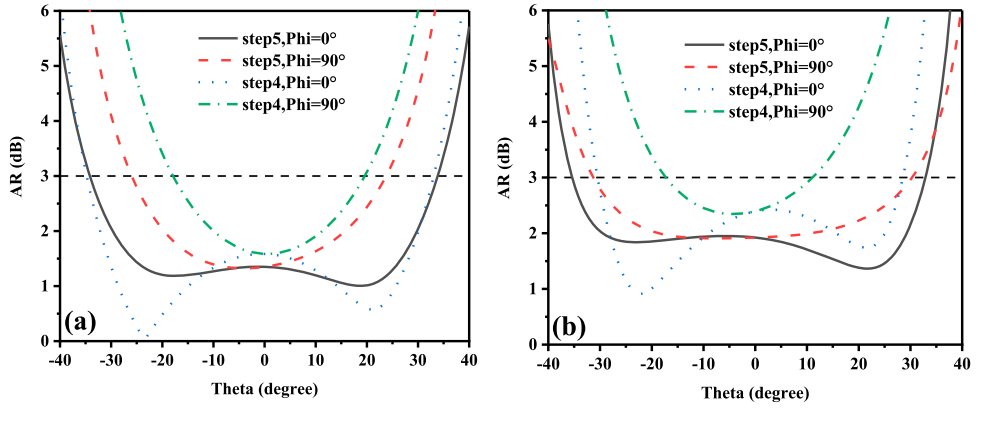

Figure 10. Simulate AR against theta: (a) 5.8 GHz, (b) 6.3 GHz.

the upper and lower plates will produce different degrees of coupling, thereby changing the amplitude. At the same time, there is little difference in impedance bandwidth between $h_3 = 6$ mm and $h_3 = 8$ mm. Figure 13(b) shows that the gain increases as the height between the two substrates decrease. When $h_3 = 6$ mm, the gain peak value is the highest. However, it can be seen from the AR comparison shown in Figure 13(c) that when

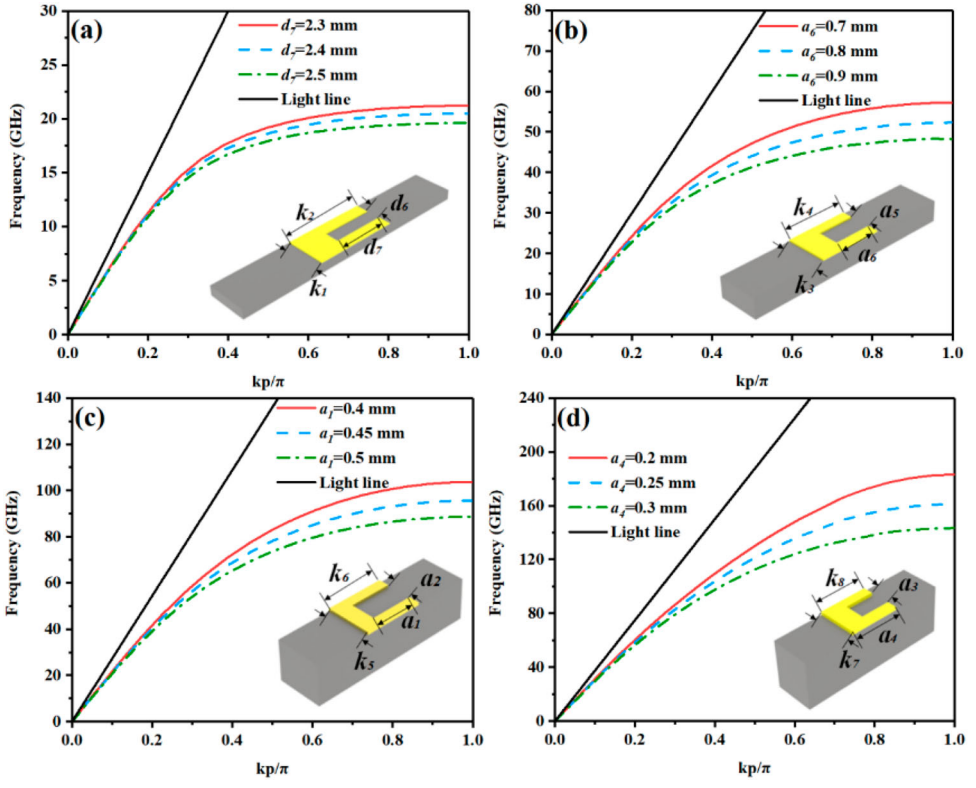

Figure 11. Dispersion diagrams of different plasmonic structures: (a) LSP, (b) SPP1, (c) SPP2, (d) SPP3.

the height between the substrates changes, the AR will also deteriorate due to the coupling between the two layers. The AR when the height of the antenna I is $h_3 = 8$ mm is the best result. When the antenna is at the height with the highest gain, that is, when $h_3 = 6$ mm, the AR value of 3.66–4.07 GHz exceeds 3 dB, which causes the bandwidth of antenna II to be 0.84 GHz narrower than that of antenna I, and the relative bandwidth deteriorates 16.6%. Although the gain is increased, the loss of AR bandwidth makes it not worthwhile.

To this end, as shown in Figure 14, spoof LSP is combined with the feed network. The zigzag-shaped periodic groove structure is used to locate the energy, which reduces the coupling between the two layers that is increased due to the short distance, thereby improving AR. Figure 15(a) shows the AR simulation results before and after the introduction of spoof LSP in the feed network. It can be seen that before the spoof LSP is added, the AR exceeds 3 dB within 3.67–4.07 GHz, the AR bandwidth is only 65.2% (4.07–7.33 GHz). After the introduction of spoof LSP, the AR simulation results are significantly improved around 4 GHz and increased to 76.6% (3.43–7.26 GHz). In addition, Figure 15(b) shows the gain simulation results before and after the introduction of spoof LSP. It can be seen that while improving the AR, the gain is also slightly improved, and the peak gain reaches 12.15 dBi.

Compared with the antenna I, the gain of antenna II is increased by 0.95 dBi, but the 3-dB ARBW will inevitably deteriorate as the gain increases. The antenna I improve the

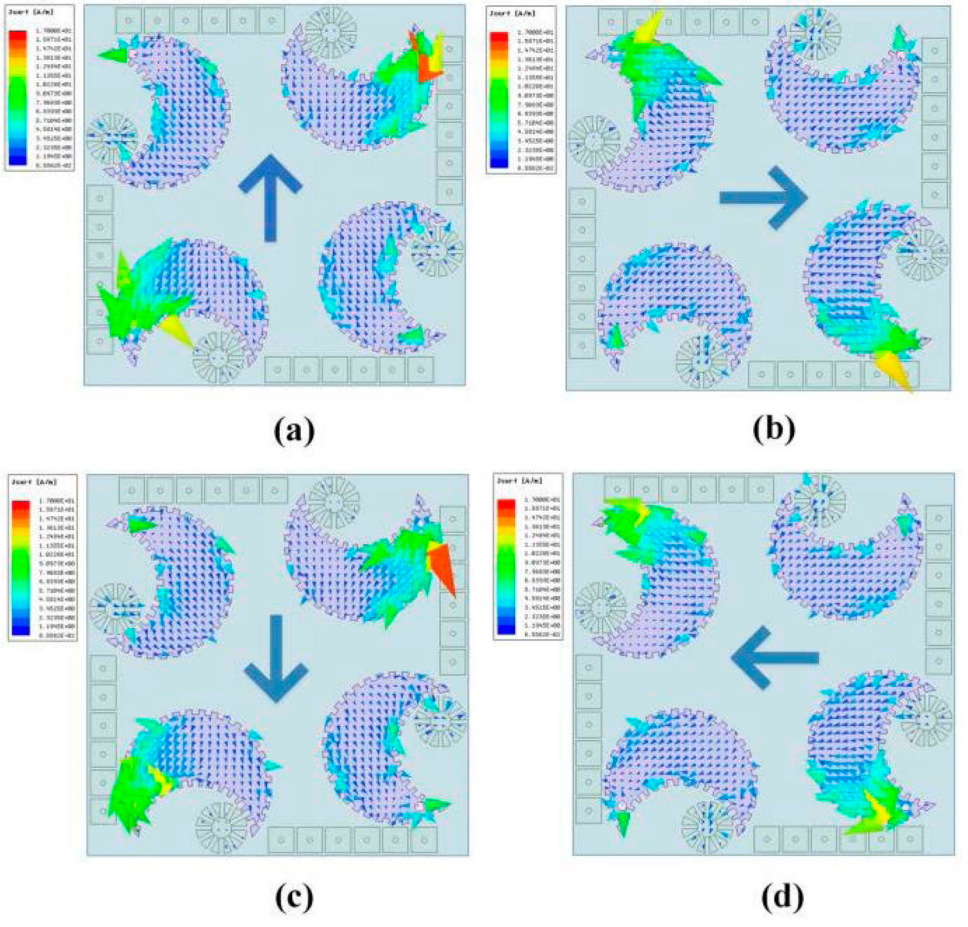

Figure 12. Antenna current distribution at 5 GHz: (a) 0°, (b) 90°, (c) 180°, (d) 270°.

3-dB ARBW while increasing the gain, and antenna II further increases the gain based on antenna I, so both are meaningful.

3. Experimental verification

To verify the simulation results, Figure 16 shows the fabricated designed antenna I and antenna II. The $|S_{11}|$ and other indicators of the antenna are measured by a vector network analyzer and a Microwave Anechoic Chamber, respectively.

3.1. Measurement of antenna I

As shown in Figure 17(a), the measured impedance bandwidth is 72% from 3.15 GHz to 6.75 GHz, which is roughly the same as the simulated impedance bandwidth. Figure 17(b) shows the measured AR bandwidth is 55% from 3.97–6.72 GHz, which is not quite the same as the simulated one. The AR value deteriorates in the low-frequency band before 4 GHz. This may be due to the limited range of probe lengths that can be selected, so

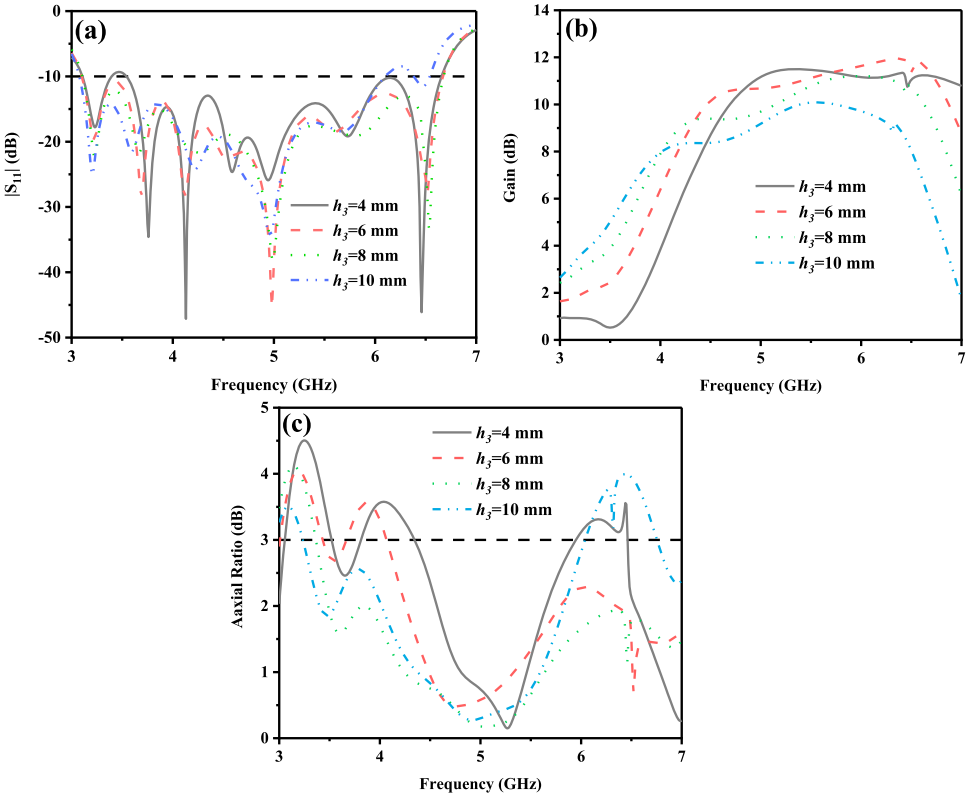

Figure 13. Simulate results for different h_3: (a) gain, (b) AR, (c) $|S_{11}|$.

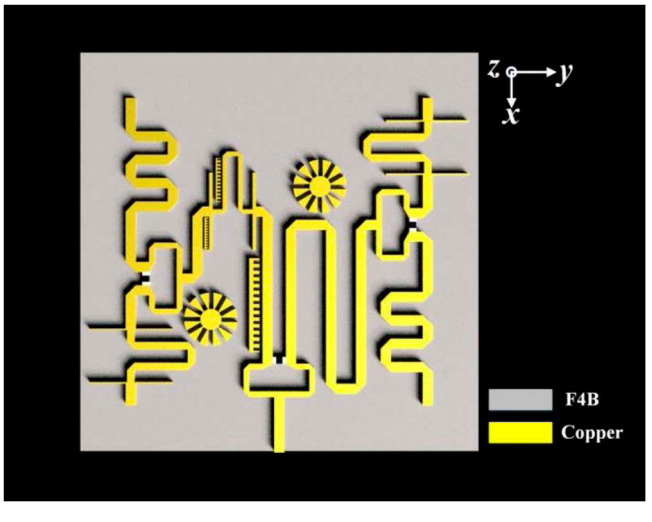

Figure 14. Geometry of the feed network with spoof LSP.

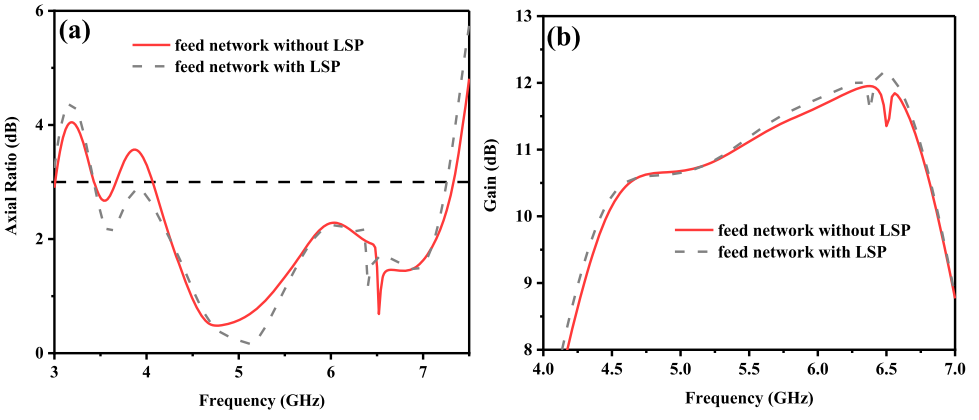

Figure 15. Comparison of feed network with and without spoof LSP: (a) AR, (b) gain.

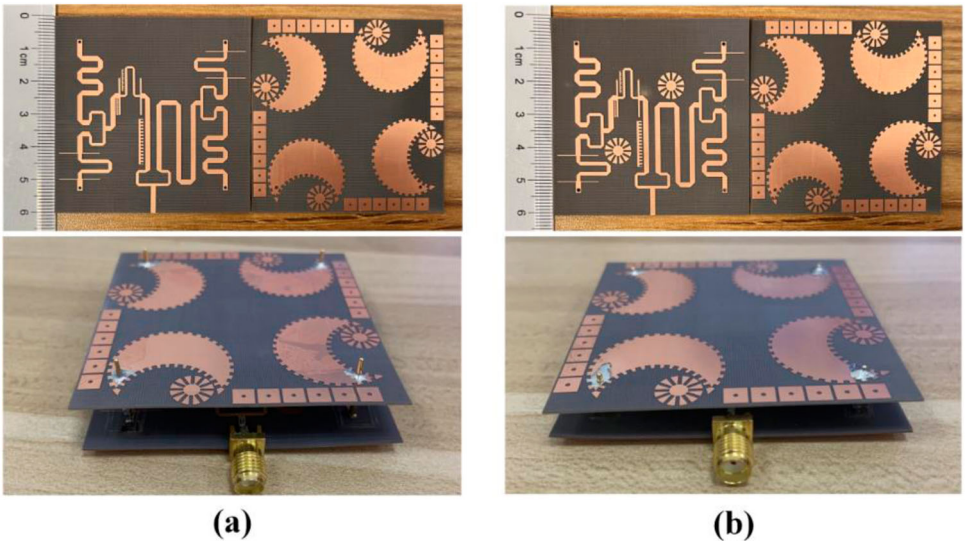

Figure 16. Photograph of the fabricated prototype: (a) antenna I, (b) antenna II.

there is an error of about 0.6 mm between the probe size used in the experiment and the simulation, and it may also be caused by welding errors. In addition, the bending of the double-layer substrate, metal oxidation and the substrate itself may all cause errors. Figure 17(c) shows the measured and simulated gain results of the antenna. It is clear that the simulated and measured results are basically consistent, and the measured peak gain is 11.11 dBi. Generally speaking, slight errors may be caused by manufacturing errors and instability in measurement. The normalized radiation patterns at 5.8 and 6.3 GHz were also measured in the actual verification, as shown in Figure 18(a,b), respectively. LHCP can be observed at the two frequency points, and the LHCP is at least 15 dB higher than the right-hand circularly polarized (RHCP) in the main polarization direction, which also verifies the existence of CP. At 5.8 GHz, the LHCP is 15 dB higher than the RHCP from −30° to

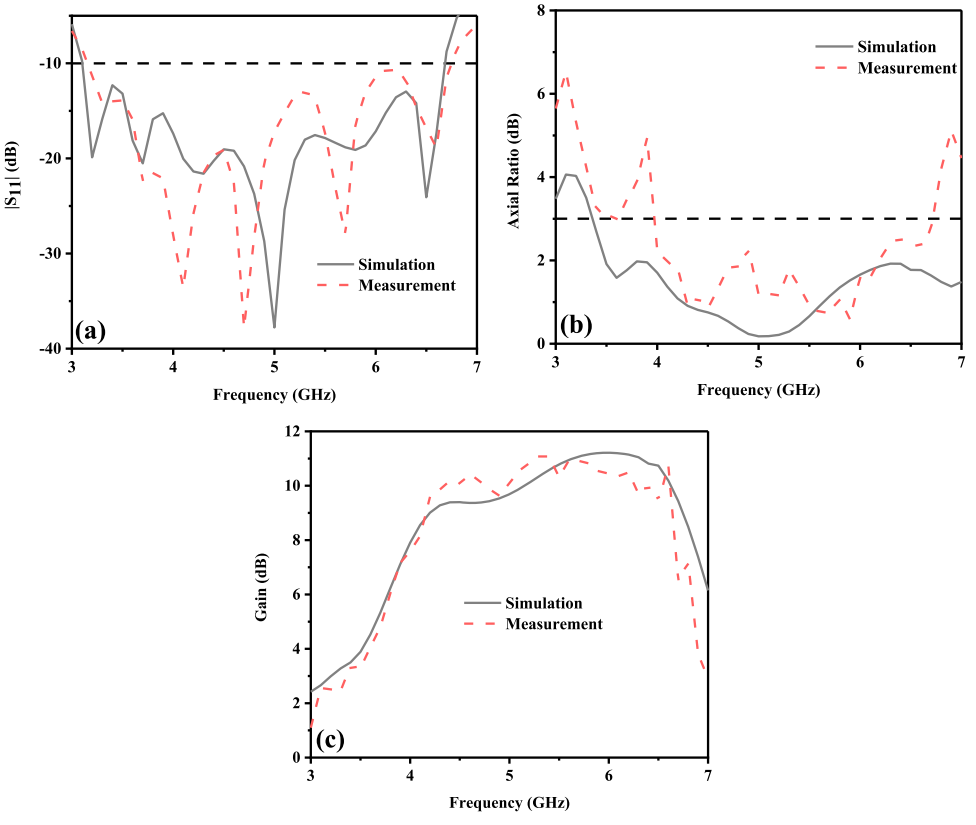

Figure 17. Comparison of measured and simulated curves of antenna I: (a) $|S_{11}|$, (b) AR, (c) gain.

26°, and at 6.3 GHz, the angle is from −15.5° to 20°. There is a slight difference between the measured and simulated results, which may be caused by the fact that the upper and lower dielectric plates are not completely parallel.

3.2. Measurement of antenna II

As shown in Figure 19(a), the simulated impedance bandwidth is 71.8% from 3.14 GHz to 6.73 GHz, which is basically the same as the simulation result. Figure 19(b) shows the measured AR bandwidth is 53.2% from 4.10 to 6.76 GHz, which is not quite the same as the simulated one. This may be due to impedance mismatch caused by parasitic capacitances generated when soldering the probes, resulting in an AR value higher than 3 dB in the low-frequency band before 4.10 GHz, which is slightly worse than the simulation results. Figure 19(c) shows the measured and simulated gain results of the antenna, and it can be seen that the overall trend of the two is basically consistent, with a measured peak gain of 12.05 dBi. The normalized radiation patterns at 5.8 and 6.3 GHz were also measured in the actual verification, as shown in Figure 20(a,b), respectively. Since the structure of the proposed antenna is relatively symmetrical, the symmetry of the radiation patterns is better. It is clear that the antenna is LHCP at both 5.8 and 6.3 GHz, the LHCP is 15 dB higher than the RHCP from −26.5° to 10.7°, and at 6.3 GHz, the angle is from −27.1° to

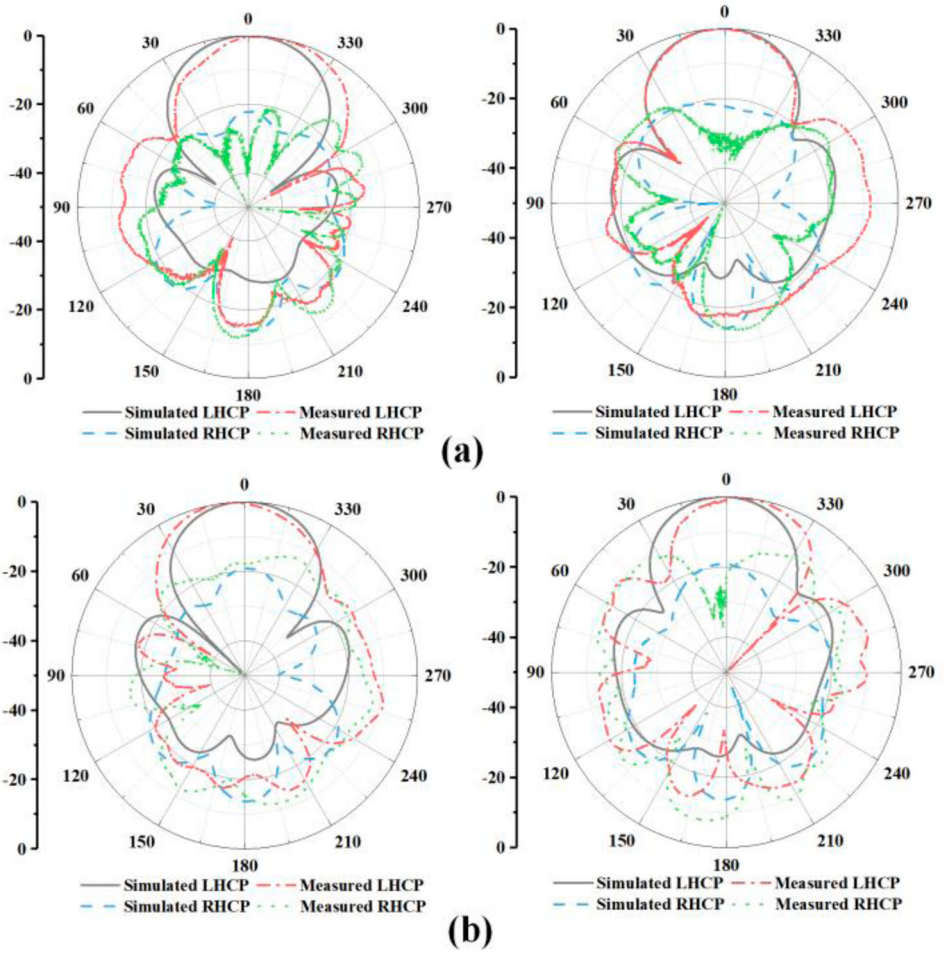

Figure 18. Normalized radiation patterns of antenna I at: (a) 5.8 GHz, (b) 6.3 GHz.

Table 3. Comparison with other antennas.

Ref.	Size (λ_g)	$\lvert S_{11}\rvert$ BW (%)	AR BW (%)	Peak gain (dBi)
[4]	$0.94 \times 0.94 \times 0.017$	100	50	7.5
[8]	$2.25 \times 1.67 \times 0.11$	72.6	69	10.38
[10]	$1.25 \times 1.88 \times 0.14$	80	62	12
Antenna I	$1.27 \times 1.27 \times 0.18$	72	55	11.11
Antenna II	$1.27 \times 1.27 \times 0.13$	71.8	52.3	12.05

22.9°. The measured results are well-matched with the simulated results. Finally, Table 3 lists the performance comparison between the antenna arrays in other references and the proposed antenna I and antenna II. It can be seen from Table 3 that the size of the antenna is smaller than that in Refs. [8,10]. Although the antenna in Ref. [4] has a smaller size, its gain is much smaller than the proposed antennas.

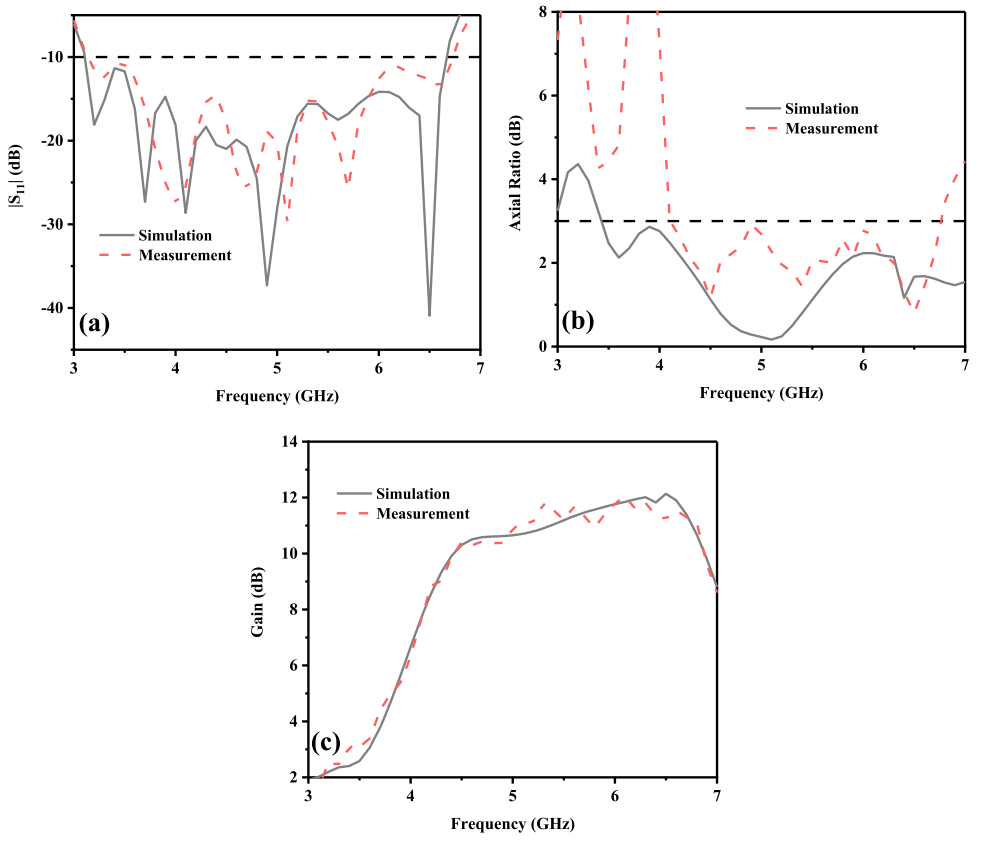

Figure 19. Comparison of measured and simulated curves of antenna II: (a) $|S_{11}|$, (b) AR, (c) gain.

4. Conclusion

Two CP 2×2 antenna arrays combined with the spoof SPP and spoof LSP are proposed in this paper. The proposed antennas use a feed network and crescent-shaped radiation patches, which effectively enhance the impedance and AR bandwidth. The antenna I combine this structure with the spoof SPP and spoof LSP, and uses periodic grooves to locate the energy to increase gain while suppressing cross-polarization. In addition, EBG is also used in this article because it can suppress surface electromagnetic waves. The antenna II adjusts the distance between the two substrates on this basis and combines the ability of the spoof LSP to restrain electromagnetic waves to reduce the coupling between the two substrates. To verify the simulation results, we fabricated the proposed antenna and measured it. The antenna I can reach 72% (3.15–6.75 GHz) measured impedance bandwidth and 55% (3.97–6.72 GHz) measured AR bandwidth, the peak gain is 11.11 dBi. Antenna II can reach 71.8% (3.14–6.73 GHz) measured impedance bandwidth and 53.2% (4.10–6.76 GHz) measured AR bandwidth, the peak gain is 12.05 dBi.

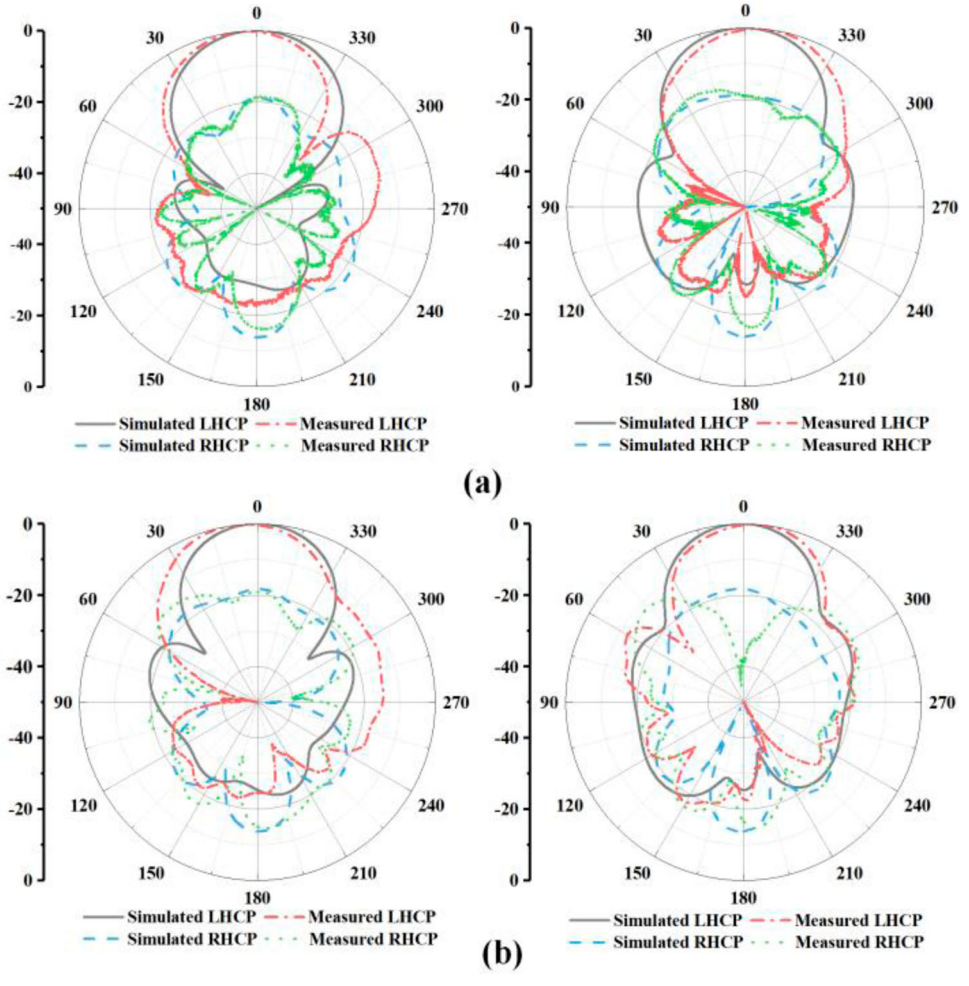

Figure 20. Normalized radiation patterns of antenna II at: (a) 5.8 GHz, (b) 6.3 GHz.

Disclosure statement

No potential conflict of interest was reported by the author(s).

References

[1] Kraft UR. An experimental study on 2×2 sequential-rotation arrays with circularly polarized microstrip radiators. IEEE Trans Antennas Propag. Oct. 1997;45(10):1459–1466. doi:10.1109/8.633850

[2] Lin S, Lin Y. A compact sequential-phase feed using uniform transmission lines for circularly polarized sequential-rotation arrays. IEEE Trans Antennas Propag. 2011;59(7):2721–2724. doi:10.1109/TAP.2011.2152346

[3] Chen A, Zhang Y, Chen Z, et al. A Ka-band high-gain circularly polarized microstrip antenna array. IEEE Antennas Wirel Propag Lett. 2010;9:1115–1118. doi:10.1109/LAWP.2010.2093866

[4] Asrin P, Hosein RM, Pejman M. Wide-band circularly polarised antenna array using sequential phase feed structure and reinforced square radiating patch element. Iet Microw Antennas Propag. 2018;12(8):1395–1399. doi:10.1049/iet-map.2017.1075

[5] Mohammadi-Asl S, Nourinia J, Ghobadi C, et al. Wideband compact circularly polarized sequentially rotated array antenna with sequential-phase feed network. IEEE Antennas Wirel Propag Lett. 2017;16:3176–3179. doi:10.1109/LAWP.2017.2767180
[6] Ding K, Gao C, Qu D, et al. Compact broadband circularly polarized antenna With Parasitic patches. IEEE Trans Antennas Propag. 2017;65(9):4854–4857. doi:10.1109/TAP.2017.2723938
[7] Zhang JD, Wu W, Fang DG. Dual-band and dual-circularly polarized shared-aperture array antennas with single-layer substrate. IEEE Trans Antennas Propag. 2016;64(1):109–116. doi:10.1109/TAP.2015.2501847
[8] Xu HF, Zhou JY, Yu ZQ, et al. Low-profile broadband circularly polarised patch antenna with gain enhancement. IET Microw Antennas Propag. 2017;11:1817–1822. doi:10.1049/iet-map.2017.0143
[9] Eom SY, Park HK. New switched-network phase shifter with broadband characteristics. Microw Opt Technol Lett. 2003;38(4):255–257. doi:10.1002/mop.11030
[10] Chung KL, Li YS, Zhang CW. Broadband artistic antenna array composed of circularly polarized Wang-shaped patch elements. AEU Arch Elektron Uebertrag Electron Commun. 2017;74:116–122. doi:10.1016/j.aeue.2017.02.006
[11] Liu Q, Chen ZN, Liu Y, et al. Compact ultra-wideband circularly-polarized weakly coupled patch array antenna. IEEE Trans Antennas Propag. 2017;65(4):2129–2134. doi:10.1109/TAP.2017.2671455
[12] Mohamed IS, Atrash ME, Abdalgalil O, et al. Wearable high gain low SAR antenna loaded with backed all-textile EBG for WBAN applications. IET Microw Antennas Propag. 2020;14(8):791–799. doi:10.1049/iet-map.2019.1089
[13] Aribi T, Naser-Moghadasi M, Sadeghzadeh RA. Circularly polarized beam-steering antenna array with enhanced characteristics using UCEBG structure. Int J Microw Wirel Technol. 2016;8(6):955–962. doi:10.1017/S1759078715000318
[14] Jam S, Malekpoor H. Compact 1∗4 patch antenna array by means of EBG structures with enhanced bandwidth. Microw Opt Technol Lett. 2016;58(12):2983–2989. doi:10.1002/mop.30197
[15] Kong GS, Ma HF, Cai BG, et al. Continuous leaky-wave scanning using periodically modulated spoof plasmonic waveguide. Rep. 2016;6: article no.29600. doi:10.1038/srep29600
[16] Hao CZ, Fan Y, Jian G, et al. Second-harmonic generation of spoof surface plasmon polaritons using nonlinear plasmonic metamaterials. ACS Photon. 2016;3(1):139–146. doi:10.1021/acsphotonics.5b00580
[17] Bai Y, Cheng A. A spoof surface plasmon leaky-wave antenna with circular polarization. Int J RF Microw Comput-Aided Eng. 2020;30(8):e22248. doi:10.1002/mmce.22248
[18] Gao X, Zhang HC, He PH, et al. Crosstalk suppression based on mode mismatch between spoof SPP transmission line and microstrip. IEEE Trans Compon Packag Manuf Technol. 2019;9(11):2267–2275. doi:10.1109/TCPMT.2019.2931373
[19] Liao Z, Pan BC, Shen X, et al. Multiple Fano resonances in spoof localized surface plasmons. Optics Expr. 2014;22(13):15710–15717. doi:10.1364/OE.22.015710
[20] Shen X, Cui TJ. Ultrathin plasmonic metamaterial for spoof localized surface plasmons. Laser Photon Rev. 2013;8(1):137–145. doi:10.1002/lpor.201300144
[21] Liao Z, Shen XP, Pan BC, et al. Combined system for efficient excitation and capture of LSP resonances and flexible control of SPP transmissions. ACS Photon 2015;2(6):738–743. doi:10.1021/acsphotonics.5b00096